American Mineralogist, Volume 109, pages 2142–2151, 2024

Three new iron-phosphate minerals from the El Ali iron meteorite, Somalia: Elaliite $Fe_8^{2+}Fe^{3+}(PO_4)O_8$, elkinstantonite $Fe_4(PO_4)_2O$, and olsenite $KFe_4(PO_4)_3$

Christopher D.K. Herd[1,*,§], Chi Ma[2,†], Andrew J. Locock[1], Radhika Saini[1], and Erin L. Walton[3,‡]

[1]Department of Earth and Atmospheric Sciences, University of Alberta, Edmonton, Alberta T6G 2R3, Canada
[2]Division of Geological and Planetary Sciences, California Institute of Technology, Pasadena, California 91125, U.S.A.
[3]Department of Physical Sciences, MacEwan University, City Centre Campus, 10700 104 Avenue, Edmonton, Alberta T5J 4S2, Canada

Abstract

Petrologic investigation of the El Ali IAB iron meteorite (Somalia) revealed three new minerals: elaliite [$Fe_8^{2+}Fe^{3+}(PO_4)O_8$, IMA 2022-087], elkinstantonite [$Fe_4(PO_4)_2O$, IMA 2022-088], and olsenite [$KFe_4(PO_4)_3$, IMA 2022-100]. The name elaliite recognizes the occurrence of this mineral within the El Ali meteorite, originally located at 4° 17′ 17″N, 44° 53′ 54″E. Elkinstantonite is named after Linda (Lindy) Elkins-Tanton (b. 1965), a planetary scientist and professor in the School of Earth and Space Exploration at Arizona State University. The name olsenite is in honor of Edward J. Olsen (1927–2020), the former Curator of Mineralogy and Meteorites at the Field Museum of Natural History in Chicago (1960–1991). The new minerals and their names have been approved by the Commission on New Minerals, Nomenclature and Classification of the International Mineralogical Association. The holotype specimens of elaliite, elkinstantonite, and olsenite consist of the polished block mount with accession number MET11814/2-1/EP1 deposited in the University of Alberta Meteorite Collection. Elaliite, elkinstantonite, and olsenite occur along with wüstite, troilite, sarcopside, and Ca-bearing graftonite within inclusions in the iron-nickel metal (kamacite, 9.4 wt% Ni) that makes up the bulk of the El Ali sample. The empirical formulas determined by electron probe microanalysis for elaliite, elkinstantonite, and olsenite are: $(Fe^{2+}_{7.943}Fe^{3+}_{1.020}Cr_{0.010}Ni_{0.006}Ca_{0.004}Mn_{0.004})_{\Sigma 8.987}(P_{0.932}Si_{0.077}S_{0.005})_{\Sigma 1.014}O_{12}$, $(Fe^{2+}_{3.947}Mn_{0.016}Ni_{0.003}Ca_{0.001}Cr_{0.001})_{\Sigma 3.968}(P_{1.986}Si_{0.014}S_{0.013})_{\Sigma 2.013}O_9$, and $(K_{0.820}Na_{0.135}Ca_{0.004})_{\Sigma 0.959}(Fe_{3.829}Mn_{0.050})_{\Sigma 3.879}(P_{2.972}S_{0.058}Si_{0.017})_{\Sigma 3.047}O_{12}$, respectively. Electron backscatter diffraction was used to confirm the crystal structures of the three new minerals. Raman spectra for all three minerals are also presented.

Keywords: New mineral, elaliite, elkinstantonite, olsenite, iron phosphate, IAB meteorite, EBSD, electron microprobe

Introduction

The El Ali meteorite is a 15.2 metric-ton iron meteorite from Somalia (Gattacceca et al. 2022), originally known by herders and others in the region as "Nightfall." The meteorite belongs to the IAB Complex group of iron meteorites. This group includes a diversity of bulk compositions as well as a high number of meteorites containing silicate or other inclusions. IAB iron-nickel meteorites may have formed by melting due to impact heating on a porous chondritic body (Wasson and Kallemeyn 2002).

Of the 12 phosphide minerals that occur in meteorites, schreibersite, $(Fe,Ni)_3P$, is the most common in IAB iron meteorites, where it is commonly found in contact with Fe-Ni metal (Rubin and Ma 2021). Phosphate minerals in IAB irons are often located within silicate inclusions (Rubin and Ma 2021).

In the course of the classification of the El Ali iron meteorite, we noted phosphate inclusions that could not be definitively identified by energy-dispersive spectrometry (EDS). More detailed study in the Electron Microprobe Laboratory at the University of Alberta and the Analytical Facility at Caltech revealed three new iron-phosphate minerals: elaliite [$Fe_8^{2+}Fe^{3+}(PO_4)O_8$, IMA 2022-087], elkinstantonite [$Fe_4(PO_4)_2O$, IMA 2022-088], and olsenite [$KFe_4(PO_4)_3$, IMA 2022-100].

The name elaliite recognizes the occurrence of this mineral within the El Ali meteorite, originally located at 4° 17′ 17″N, 44° 53′ 54″E. The meteorite, described in 2021 (Meteoritical Bulletin Database, entry for El Ali: https://www.lpi.usra.edu/meteor/metbull.php?code=74444), is named after the nearby town of El Ali (Somali: Ceel Cali), Hiiraan region, Somalia (Appendix S1 of Gattacceca et al. 2022). The local herders report that they have known of this rock for more than 5–7 generations, and that it is memorialized through Saar folklore, songs, dances, and poems.

Elkinstantonite is named after Linda (Lindy) Elkins-Tanton (b. 1965), a planetary scientist and professor in the School of Earth and Space Exploration at Arizona State University. Elkins-Tanton is an expert in the chemistry and physics of the formation of the terrestrial planets, and she has made pivotal contributions to our understanding of the differentiation of rocky planets, the formation of planetary cores and magma oceans, the degassing of planetary atmospheres, and the delivery of water to the early Earth. She is the Principal Investigator of the NASA Psyche

* Corresponding author E-mail: herd@ualberta.ca. Orcid https://orcid.org/0000-0001-5210-4002
† Orcid https://orcid.org/0000-0002-1828-7033
‡ Deceased September 21, 2022.

mission, a mission to explore the metallic asteroid—and possible core of a protoplanet—16 Psyche. The mineral name honors Lindy's influence on the field of planetary core formation.

The name olsenite is in honor of Edward J. Olsen (1927–2020), the former Curator of Mineralogy and Meteorites at the Field Museum of Natural History in Chicago (1960–1991), who helped describe several new minerals from meteorites: brianite, buchwaldite, galileiite, krinovite, and panethite, and who was the first to find phosphate minerals in iron meteorites (Steele and Hutcheon 2020).

The new minerals and their names have been approved by the Commission on New Minerals, Nomenclature and Classification of the International Mineralogical Association. The holotype specimens of elaliite, elkinstantonite, and olsenite consist of the polished block mount with accession number MET11814/2-1/EP1 deposited in the University of Alberta Meteorite Collection.

Experimental methods

Examination by scanning electron microscopy was undertaken both at the University of Alberta (Zeiss Sigma 300 variable-pressure field-emission scanning electron microscope, VP-FE-SEM, operated at 15 kV accelerating voltage), and Caltech (Zeiss 1550VP FE-SEM, operated at 10 kV). Both backscattered-electron images and energy-dispersive X-ray spectra were acquired.

For elaliite and elkinstantonite, a Cameca SX100 electron microprobe at the University of Alberta was used to examine the polished and carbon-coated (25 nm thickness) epoxy mount MET11814/2-1/EP1. Quantitative data for 12 elements (Na, Mg, Si, P, S, K, Ca, Cr, Mn, Fe, Ni, and Sr) were acquired using wavelength-dispersive spectrometry (WDS) and Probe for EPMA software (Donovan et al. 2015), with operating conditions: 15 kV accelerating voltage, 20 to 30 nA probe current, and <1 μm beam diameter. Total count times of 30 s were used for both peaks and backgrounds. The X-ray lines, diffraction crystals, and standards were: Na*K*α, TAP (thallium hydrogen phthalate), tugtupite; Mg*K*α, TAP, diopside; Si*K*α, TAP, diopside; P*K*α, PET (pentaerythritol), fluorapatite; S*K*α, PET, anhydrite; K*K*α, PET, sanidine; Ca*K*α, PET, fluorapatite; Cr*K*α, PET, synthetic Cr_2O_3; Mn*K*α, LIF (lithium fluoride), spessartine; Fe*K*α, LIF, fayalite; Ni*K*α, LIF, nickel metal; and Sr *L*α, PET, synthetic $SrTiO_3$. Time-dependent intensity corrections for Na, P, K, Ca, and Fe were carried out (peak count times divided into six intervals) with Probe for EPMA software following Nielsen and Sigurdsson (1981). X-ray data were reduced following Armstrong (1995). The stoichiometric proportions of ferric iron for elaliite analyses were calculated (on the basis of 10 cations and 12 anions) and included in the iterated matrix corrections with the Probe for EPMA software (Droop 1987; Dungan et al. 2023). The following constituents were sought by WDS but did not yield average results above the limits of detection (wt%): Na_2O (0.02), K_2O (0.02), MgO (0.02), and SrO (0.06). No other elements with Z >10 were observed by EDS.

For olsenite, a JEOL 8900R electron microprobe at the University of Alberta was used to examine the polished and carbon-coated (25 nm thickness) epoxy mount MET11814/2-1/EP1. Quantitative data for 11 elements (Na, Mg, Si, P, S,

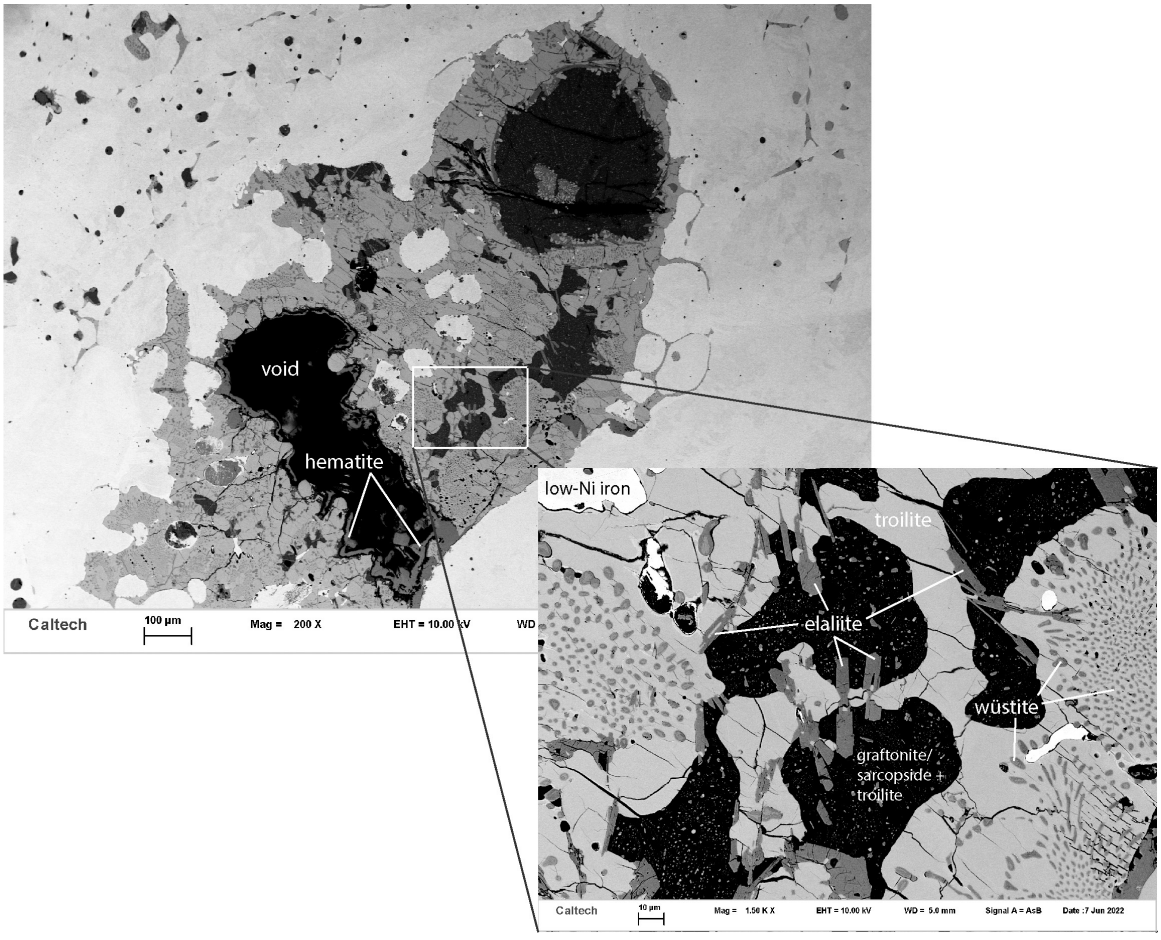

Figure 1. Backscattered electron image of a large inclusion in the El Ali meteorite (including void and hematite interpreted to be from terrestrial alteration). Inset shows elongate crystals of elaliite (medium gray) in a sarcopside/graftonite-rich cavity (dark gray), surrounded by troilite with a symplectic intergrowth of wüstite (light gray, and medium-light gray, respectively), and low-Ni iron (white).

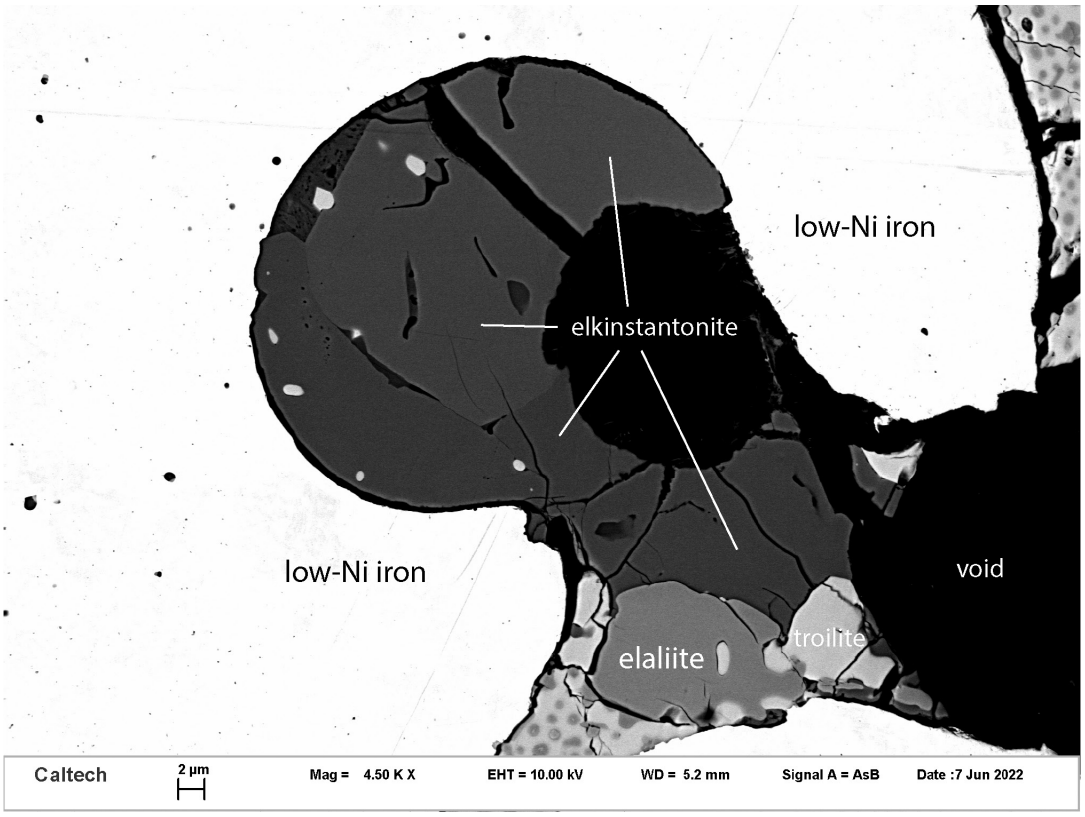

Figure 2. Backscattered electron image of elkinstantonite (dark gray) in low-Ni iron (white) with elaliite (medium gray) and troilite (light gray). Slight differences in grayscale within elkinstantonite are likely caused by minor compositional variations (observed by FE-SEM-EDS).

K, Ca, Cr, Mn, Fe, Ni) were acquired using wavelength-dispersive spectrometry (WDS) and Probe for EPMA software (Donovan et al. 2015), with operating conditions: 10 kV accelerating voltage, 10 nA probe current, and <1 µm beam diameter. The lower beam energy was chosen to minimize the interaction volume and help improve the spatial resolution. Total count times of 30 s were used for both peaks and backgrounds. The X-ray lines, diffraction crystals, and standards were the same as those used for elaliite and elkinstantonite, except that Sr was not sought, and the intensity data for both P and for S were each aggregated from two spectrometers (Donovan et al. 2011). Time-dependent intensity corrections for Na, P, K, and Fe were carried out (peak count times divided into six intervals) with Probe for EPMA software following Nielsen and Sigurdsson (1981). X-ray data were reduced following Armstrong (1995). The following constituents were sought by WDS but did not yield average results above the limits of detection (wt%): MgO (0.02), Cr_2O_3 (0.16), and NiO (0.35). No other elements with Z >10 were observed by EDS.

Electron backscatter diffraction (EBSD) analyses were performed using an HKL EBSD system on the Zeiss 1550VP FE-SEM at Caltech, operated at 20 kV and 6 nA in focused beam mode with a 70° tilted stage and in a variable pressure mode (25 Pa), using the method described in Ma and Rossman (2008, 2009). The focused electron beam is several nanometers in diameter. The spatial resolution for diffracted backscattered electrons is ~30 nm. The EBSD system was calibrated using a single-crystal silicon standard. Identifications and unit-cell dimensions were obtained by matching the experimental EBSD patterns with structures of Fe-P-O (-Ca or -K) phases from the Inorganic Crystal Structure Database (Hellenbrandt 2004).

Raman spectra were acquired for elaliite, elkinstantonite, and olsenite with a Horiba Xplora Plus Raman Spectrometer. A confocal Raman microscope was used to focus the beam of alternately 532 and 785 nm diode laser (~1 mW), and the 100× objective was used to obtain a laser spot diameter of 1 µm (theoretically 800 nm). Data acquisition was 1 to 5 min per spectrum (2 s dwell, with 8 accumulations). The spectra were recorded in the range 1500–50 cm^{-1}. Peak positions were calibrated using a silicon wafer and peak fitting was conducted using the Labspec 6 spectroscopy-suite software.

Results

Occurrence

Elaliite, elkinstantonite, and olsenite occur along with wüstite, troilite, sarcopside, and Ca-bearing graftonite within inclusions in the iron-nickel metal (kamacite, 9.4 wt% Ni) that makes up the bulk of El Ali (Figs. 1–3). Most inclusions are ~100 µm across, although larger, millimeter-scale inclusions have the greatest mineralogical diversity. In larger inclusions, elaliite typically occurs as ~10 × 50 µm euhedral, elongate laths at the interfaces of troilite and/or wüstite and graftonite-rich areas (Fig. 1). Graftonite-rich areas also contain <5 µm grains of Si-bearing sarcopside, elaliite, and troilite (Fig. 1). In smaller (<200 µm) inclusions, elaliite occurs with troilite set in a matrix of sarcopside or graftonite (Fig. 2); this is also the typical setting for olsenite (Fig. 3). Elkinstantonite has thus far only been found in a smaller inclusion, as subhedral grains associated with troilite and wüstite symplectites, troilite, and elaliite (Fig. 2). Minor terrestrial alteration extends along fractures and grain boundaries, which is consistent with the specimen being taken from the exterior of the meteorite (Fig. 1).

Appearance, physical and optical properties

Elaliite occurs as elongate laths mainly from 1 × 5 µm to 7 × 20 µm in size (Fig. 1) and is dark brown in color. Elkinstantonite occurs as equant grains, ~10 to 20 µm in size (Fig. 2), and is transparent with a light brown color. Olsenite occurs as irregular crystals, 1 to 5 µm in size (Fig. 3); its color was not observed. As

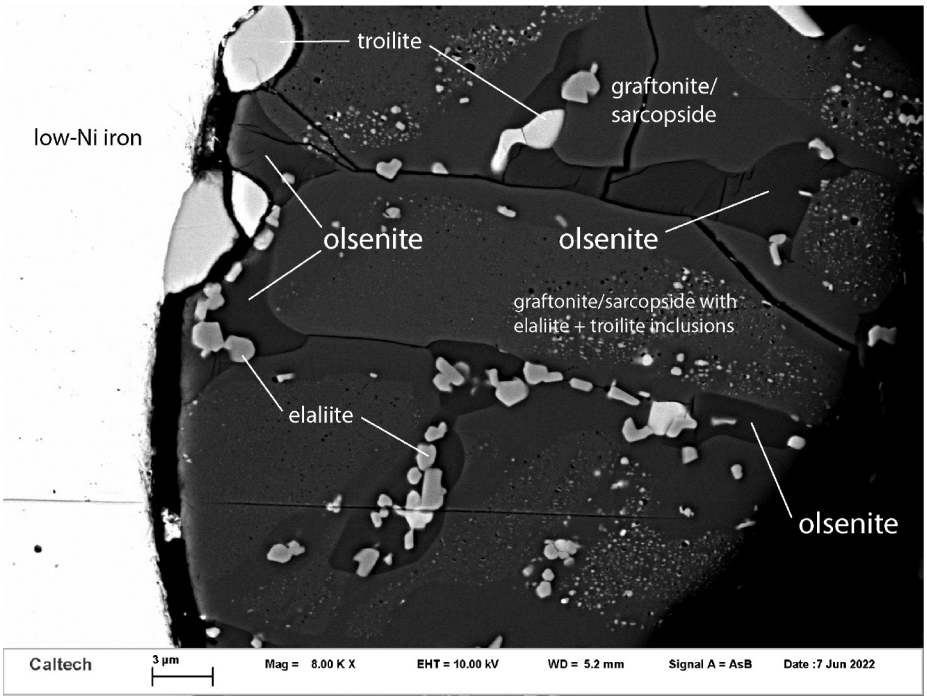

FIGURE 3. Backscattered electron image of olsenite (dark gray) with graftonite (medium gray), elaliite (light gray), troilite (very light gray), and low-Ni iron (white).

a result of their small grain sizes, optical properties and several physical properties of these minerals were not observed (including: streak, luster, Mohs hardness, cleavage, parting, tenacity, fracture, and measured density). Micro-hardness and reflectance measurements were not undertaken. These three minerals did not show visible cathodoluminescence.

Chemical compositions

The chemical compositions (mean, standard deviation, range) of elaliite, elkinstantonite, and olsenite measured by electron probe microanalysis are presented in Table 1. These analyses show the empirical formulas for elaliite, elkinstantonite, and olsenite (respectively) to be: $(Fe^{2+}_{7.943}Fe^{3+}_{1.020}Cr_{0.010}Ni_{0.006}Ca_{0.004}Mn_{0.004})_{\Sigma 8.987}(P_{0.932}Si_{0.077}S_{0.005})_{\Sigma 1.014}O_{12}$, $(Fe^{2+}_{3.947}Mn_{0.016}Ni_{0.003}Ca_{0.001}Cr_{0.001})_{\Sigma 3.968}(P_{1.986}Si_{0.014}S_{0.013})_{\Sigma 2.013}O_9$, and $(K_{0.820}Na_{0.135}Ca_{0.004})_{\Sigma 0.959}(Fe_{3.829}Mn_{0.050})_{\Sigma 3.879}(P_{2.972}S_{0.058}Si_{0.017})_{\Sigma 3.047}O_{12}$, respectively. The ideal formulas of elaliite, elkinstantonite, and olsenite are $Fe^{2+}_8Fe^{3+}(PO_4)O_8$, $Fe_4(PO_4)_2O$, and $KFe_4(PO_4)_3$, respectively, which require (each sum 100.00 wt%): elaliite = P_2O_5 9.78, FeO 79.22, and Fe_2O_3 11.00 wt%; elkinstantonite = P_2O_5 33.06, and FeO 66.94 wt%; and olsenite = K_2O 8.60, FeO 52.50, P_2O_5 38.90 wt%.

Crystallography and structures

Electron backscatter diffraction was used to confirm the crystal structures of the three new minerals. Chemistry-limited searches of the Inorganic Crystal Structure Database (Hellenbrandt 2004) yielded excellent matches to synthetic materials: elaliite = $Fe_9(PO_4)O_8$, Venturini et al. (1984), mean angular deviation 0.32 to 0.37° (Fig. 4); elkinstantonite = $Fe_4(PO_4)_2O$, Bouchdoug et al. (1982), mean angular deviation 0.22 to 0.36° (Fig. 5); and olsenite = $KFe_4(PO_4)_3$, Matvienko et al. (1981), mean angular deviation 0.44 to 0.48° (Fig. 6). From the unit-cell

TABLE 1. Electron microprobe analyses of elaliite, elkinstantonite, and olsenite (standard deviations in parentheses)

Mineral constituent	Elaliite Mean	n = 28 Range	Elkinstantonite Mean	n = 5 Range	Olsenite Mean	n = 5 Range	Olsenite normalized
Na_2O					0.74 (0.09)	0.66–0.89	0.78
SiO_2	0.64 (0.25)	0–1.24	0.20 (0.16)	0.08–0.47	0.18 (0.03)	0.15–0.20	0.19
P_2O_5	9.16 (0.37)	8.39–9.95	32.91 (0.51)	32.31–33.18	37.32 (0.49)	36.48–37.63	39.19
SO_3	0.06 (0.21)	0–1.11	0.24 (0.26)	0.06–0.67	0.83 (0.33)	0.65–1.42	0.87
K_2O					6.83 (0.44)	6.39–7.46	7.17
CaO	0.03 (0.03)	0–0.10	0.01 (0.01)	0–0.03	0.04 (0.06)	0–0.12	0.04
Cr_2O_3	0.10 (0.13)	0–0.45	0.01 (0.01)	0–0.03			
MnO	0.04 (0.02)	0–0.12	0.26 (0.02)	0.23–0.29	0.63 (0.08)	0.53–0.74	0.66
FeO_{total}			66.21 (0.49)	65.63–66.90	48.67 (2.32)	46.54 –52.61	51.10
FeO[a]	79.07 (0.72)	77.90–80.66					
Fe_2O_3[a]	11.26 (0.77)	9.08–12.40					
NiO	0.06 (0.06)	0–0.21	0.06 (0.02)	0.04–0.09			
Total[b]	100.42 (0.55)	99.19–101.28	99.90 (0.78)	98.81–100.97	95.24 (2.60)	93.07–99.57	

Notes: Individual values of the reported constituents that were below the limits of detection have been set to zero. Constituents whose average results were not above the limit of detection are omitted.

[a] Proportions of ferric- and ferrous-iron for elaliite calculated on the basis of 10 cations and 12 anions.

[b] The low average total of olsenite is ascribed to its grain size, micro-fractures, and surface finish (Fig. 3).

parameters determined by EBSD (Table 2), the densities were calculated (from the empirical formulas and EBSD unit-cell volumes), along with the mean refractive indices given by the Gladstone-Dale relationship (Mandarino 1976).

The crystal structure of synthetic $Fe_9(PO_4)O_8$, equivalent to elaliite, was reported by Venturini et al. (1984) to have site-

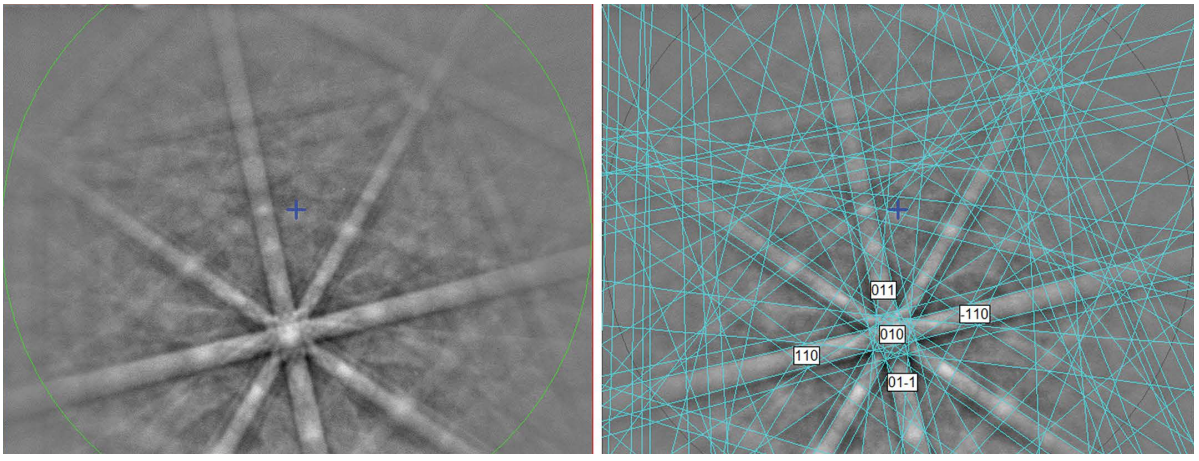

FIGURE 4. EBSD pattern of elaliite (left), indexed (right) in space group *Cmmm* based on the structure of Venturini et al. (1984). (Color online.)

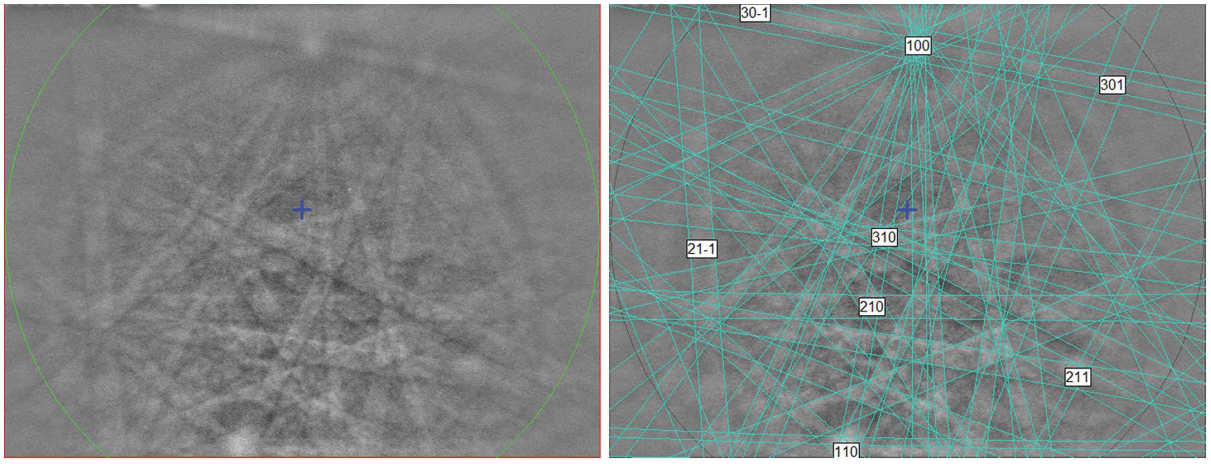

FIGURE 5. EBSD pattern of elkinstantonite (left), indexed (right) in space group $P2_1/c$ based on the structure of Bouchdoug et al. (1982). (Color online.)

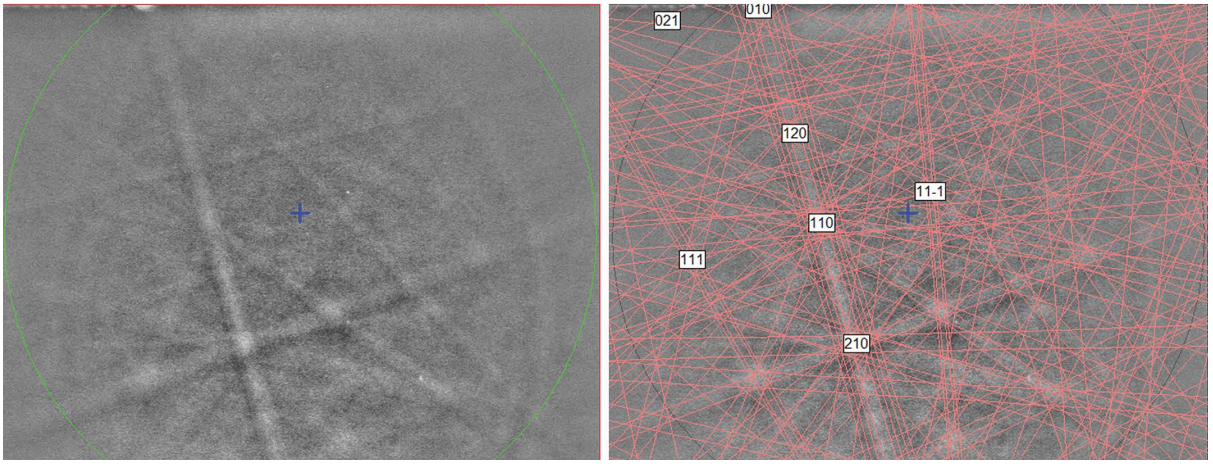

FIGURE 6. EBSD pattern of olsenite (left), indexed (right) in space group *Pnnm* based on the structure of Matvienko et al. (1981). (Color online.)

TABLE 2. Crystallographic parameters and calculated physical properties (standard deviations in parentheses) of elaliite, elkinstantonite, and olsenite

Mineral	Elaliite	Elkinstantonite	Olsenite
a (Å)	5.95 (0.01)	6.56 (0.01)	9.81 (0.01)
b (Å)	25.69 (0.01)	11.27 (0.01)	16.51 (0.01)
c (Å)	3.06 (0.01)	9.38 (0.01)	6.27 (0.01)
β (°)	90	104.0 (0.1)	90
V (Å^3)	468(2)	673(2)	1016(2)
Z	2	4	4
Space group	*Cmmm* (#65)	$P2_1/c$ (#14)	*Pnnm* (#58)
D_{calc} (g·cm^{-3})	5.15	4.22	3.52
Mean refractive index n_{calc}	2.04	1.78	1.66
Structure reference	Venturini et al. (1984)	Bouchdoug et al. (1982)	Matvienko et al. (1981)

occupancy disorder on the tetrahedral position between P and Fe^{2+}, and two of the oxygen positions are positionally disordered; it is probable that an unresolved superstructure is present. Elaliite is isotypic with $Mg_7Ga_2GeO_{12}$ and $(Mg,Ga)_8(Ga,Ge)_2O_{12}$ (Barbier and Hyde 1987; Barbier and Frampton 1992). This structure-type has been described (Barbier and Hyde 1987) as an intergrowth between the wüstite (halite structure) and β-Ga_2O_3 structures (Fig. 7).

The crystal structure of synthetic $Fe_4(PO_4)_2O$, equivalent to elkinstantonite, was reported by Bouchdoug et al. (1982). This structure consists of a dense framework of edge- and corner-sharing Fe^{2+}-centered octahedra and five-coordinated Fe^{2+}-centered polyhedra, which is further connected by phosphate tetrahedra that share edges and corners with the various Fe^{2+}-centered polyhedra (Fig. 8). The analogous copper oxyphosphate and copper oxyarsenate compounds, $Cu_4(PO_4)_2O$ and $Cu_4(AsO_4)_2O$, both occur in triclinic and orthorhombic polymorphs that differ structurally from elkinstantonite (Anderson et al. 1978; Brunel-Laügt et al. 1978; Schwunck et al. 1998; Pekov et al. 2014; Volkova 2023). The copper oxyarsenates have been described as the minerals ericlaxmanite (triclinic) and kozyrevskite (Pekov et al. 2014).

The crystal structure of synthetic $KFe_4(PO_4)_3$, equivalent to olsenite, was reported by Matvienko et al. (1981). This structure-type has been described (Sugiyama and Kimiyama 2009) as a framework that consists of buckled slabs of Fe^{2+}-centered octahedra and phosphate tetrahedra that are further linked through five-coordinated Fe^{2+}-centered polyhedra and phosphate tetrahedra, with channels that run parallel to [100] (Fig. 9). Several isotypic compounds have been reported, e.g., $KCo_3Fe(PO_4)_3$ (Assaaoudi et al. 2006); several of these are reviewed in Yakubovich et al. (2018). Olsenite is not structurally related to the minerals of the alluaudite supergroup or the fillowite group, despite similarities in their stoichiometries (Hatert 2019; Hatert et al. 2021; Tait et al. 2021). Rather, according to Britvin et al. (2020), the structure-type of olsenite is a derivative of the α-$CrPO_4$ type (Attfield et al. 1988).

Raman spectroscopy

The Raman spectra of elaliite, elkinstantonite, and olsenite acquired at both 532 and 785 nm are in good agreement, confirming that the observed bands are indeed Raman signals and not artifacts or fluorescent signals. Each of the spectra shows P-O stretching modes between 930 and 1020 cm^{-1}, out-of-plane bending modes between 450 and 650 cm^{-1}, in-plane bending modes (for elkinstantonite) around 400 cm^{-1}, and lattice modes below 250 cm^{-1} (compare Frost et al. 2002; Litasov and Podgornykh 2017; Pieczka et al. 2018) (Figs. 10–12). The Raman spectrum of elaliite has a single P-O symmetric stretching mode at 937 cm^{-1}, a broad hump centered around 488 cm^{-1}, and various lattice modes whose positions show variation among different grains (Fig. 10). Elaliite was found to be very sensitive to laser damage, consistent with potential oxidation, as is observed in Fe-oxide and sulfide minerals (de Faria et al. 1997; Fries and Steele

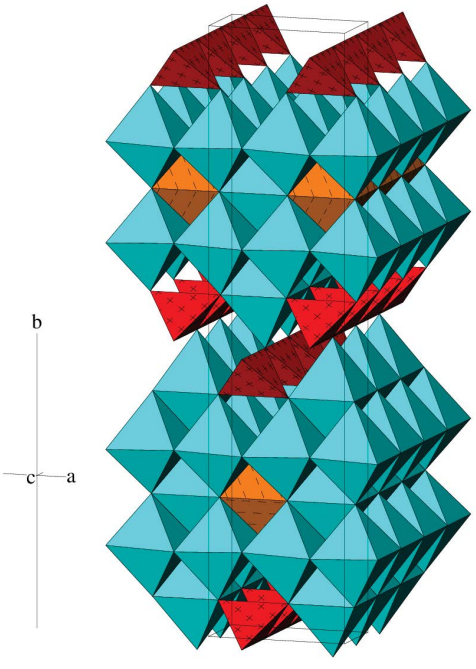

FIGURE 7. Clinographic projection of the crystal structure of elaliite in the *Cmmm* setting, after Venturini et al. (1984). The Fe^{2+}-centered octahedra are shown in blue, the Fe^{3+}-centered octahedra in orange with dashes, and the tetrahedra in red with crosses. (Color online.)

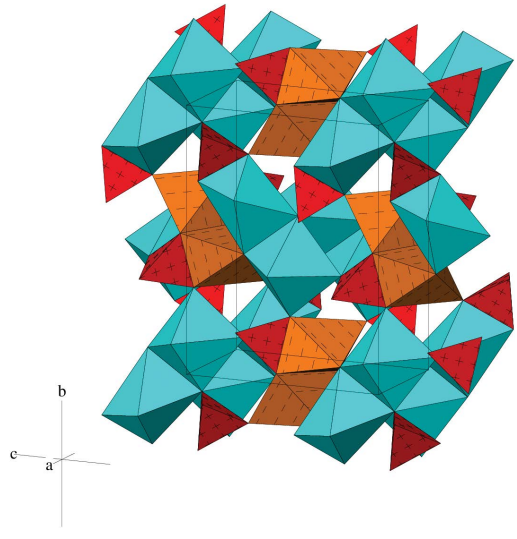

FIGURE 8. Clinographic projection of the crystal structure of elkinstantonite, after Bouchdoug et al. (1982). The Fe^{2+}-centered octahedra are shown in blue, the five-coordinated Fe^{2+}-centered polyhedra in orange with dashes, and the phosphate tetrahedra in red with crosses. (Color online.)

2018). The Raman spectrum of elkinstantonite has a triplet in the P-O symmetric stretching region at 930, 942, and 976 cm^{-1}, and a weak band at 1016 cm^{-1}, with other weak bands between 450 and 650 cm^{-1}, and lattice modes whose positions show variation among different grains (Fig. 11). The Raman spectrum of olsenite has a single symmetric stretching mode at 968 cm^{-1} and a weak band around 648 cm^{-1}; no lattice modes were resolved for the Raman spectrum of olsenite (Fig. 12). The Raman spectrum of each mineral is superimposed on a fluorescent background that differs for each mineral. The low relative peak intensities of the Raman bands, especially in the spectrum of elaliite, arise from the deliberate use of low laser power during acquisition to mitigate sample damage.

Discussion

Relationship to other species

There are at least five other iron-bearing oxyphosphate mineral species reported—beershevaite [$CaFe_3(PO_4)_3O$], crocobelonite [$CaFe_2(PO_4)_2O$], grattarolaite [$Fe_3(PO_4)O_3$], moabite [$NiFe(PO_4)O$], and staněkite [$FeMn(PO_4)O$]—all of which have Fe^{3+} as the dominant oxidation state of iron, and most of which occur in pyrometamorphic rocks (Cipriani et al. 1997; Britvin et al. 2021a, 2021b, 2023); staněkite occurs in a pegmatite (Keller et al. 1997). Elaliite and elkinstantonite are the only natural oxyphosphates that contain Fe^{2+} as the dominant oxidation state of iron, and which occur in iron meteorites. All of the iron oxyphosphate minerals (except perhaps staněkite), therefore, appear to have formed at relatively high temperatures, regardless of their differing parageneses. In the Dana classification,

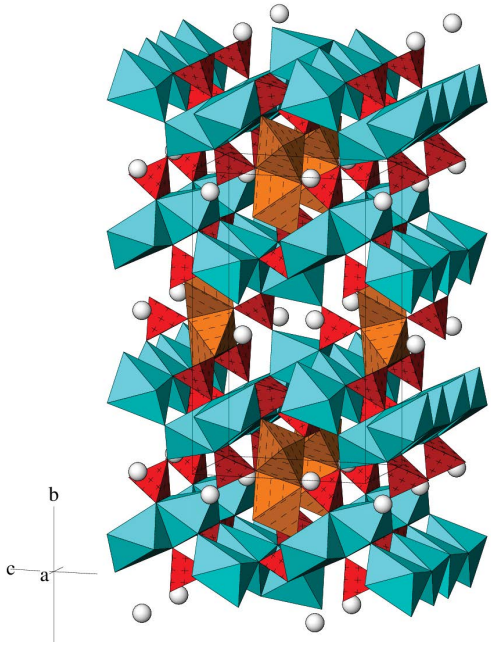

Figure 9. Clinographic projection of the crystal structure of olsenite in the *Pnnm* setting, after Matvienko et al. (1981). The Fe^{2+}-centered octahedra are shown in blue, the five-coordinated Fe^{2+}-centered polyhedra in orange with dashes, the phosphate tetrahedra in red with crosses, and the potassium atoms in gray. (Color online.)

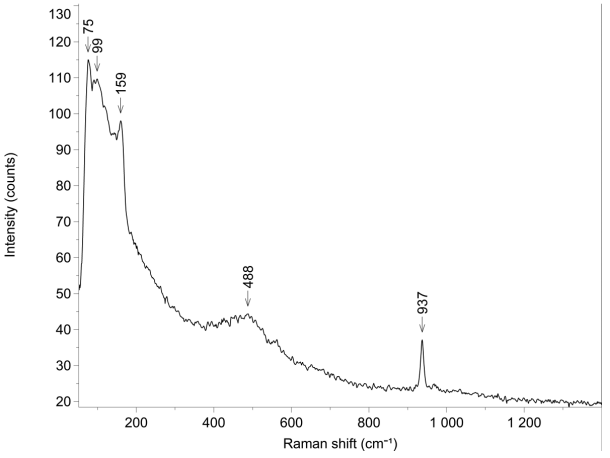

Figure 10. Raman spectrum of elaliite acquired with 532 nm wavelength radiation.

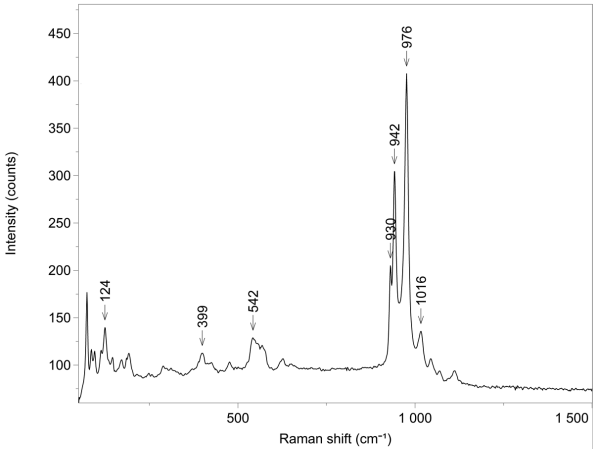

Figure 11. Raman spectrum of elkinstantonite acquired with 532 nm wavelength radiation.

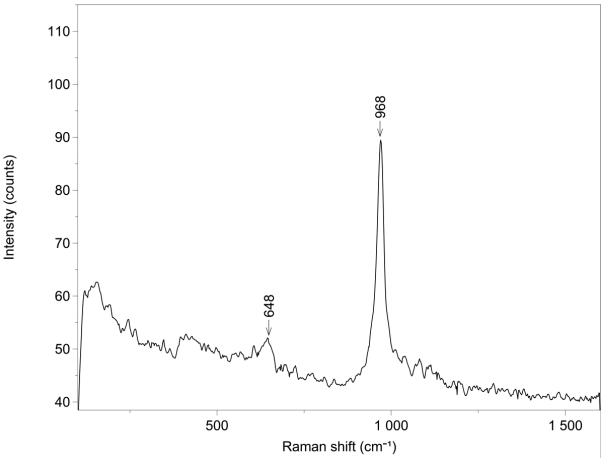

Figure 12. Raman spectrum of olsenite acquired with 532 nm wavelength radiation.

elaliite and elkinstantonite both belong to the "Anhydrous Phosphates with miscellaneous formulas," and they are most closely related (compositionally) to grattarolaite (Dana number is 38.05.12.01). In the Nickel-Strunz classification, grattarolaite similarly belongs to "Phosphates without additional anions and without H_2O and with only medium-sized cations and RO_4 >2:1" and its Nickel-Strunz number is 08.BE.10 (webmineral.com; accessed June 2022).

The formula of olsenite, $KFe_4(PO_4)_3$ is analogous to that of the alluaudite group of monoclinic phosphates and arsenates, whose general formula can be simplified for comparative purposes to $A_2M_3(TO_4)_3$ (Tait et al. 2021), where A = Na, Ca, Cu, or □; M = Na, Mg, Ca, Mn, Fe^{2+}, Fe^{3+}, Cu, Zn, or Cd; and T = P or As. The fillowite group of rhombohedral phosphates also has compositional similarities, with the simplified formula $Na_3CaC_{11}(PO_4)_9$ (Hatert et al. 2021), in which C = Mg, Mn, or Fe^{2+} for chladniite, fillowite, and johnsomervilleite, respectively. The mineral galileiite, $NaFe_4(PO_4)_3$, which is the sodium analog of olsenite, has been commonly attributed to the fillowite group because the majority of galileiite's X-ray diffraction lines (measured with a Gandolfi camera) could be indexed to a fillowite-type unit cell; the crystal structure of natural galileiite has not yet been determined. A synthetic hypersodic analog of galileiite, $Na_xFe_4(PO_4)_3$ with ($1.1 \leq x \leq 1.2$) has been reported with a monoclinic structure that is isotypic with synthetic $NaCo_4(PO_4)_3$ (Baies et al. 2006; Zhang et al. 2018). Olsen and Steele (1997) concluded that the fillowite-type unit cell interpreted from the XRD results for galileiite is not entirely satisfactory because the *d*-spacing of the 024 reflection (rhombohedral indexing), which has 40% relative intensity, shows a large difference from the calculated value: d_{obs} 5.83 vs. d_{calc} 5.51 Å. It may be notable that synthetic $Na_xFe_4(PO_4)_3$ (space group $P2_1/n$, a 6.369, b 9.950, c 15.666 Å, β 91.927°) has its calculated 101 reflection, with relative intensity 100%, at 5.829 Å (Zhang et al. 2018). The diffraction lines of galileiite (from 5.83 to 1.48 Å) found in the Grant IIB meteorite and reported by Olsen and Steele (1997) in their Table 2 can be re-indexed to yield: a = 6.38, b = 9.92, c = 15.57 Å, β = 92.0°, using the programs PowderCell and UnitCell (Kraus and Nolze 1996; Holland and Redfern 1997), based on the structure of Zhang et al. (2018). The monoclinic structure of $Na_xFe_4(PO_4)_3$ and $NaCo_4(PO_4)_3$ is related to the orthorhombic structure of olsenite and its isotypes (Yakubovich et al. 2018), which in turn is derivative from the α-$CrPO_4$ type (Attfield et al. 1988).

In the original description of galileiite, Olsen and Steele (1997) mention that "[an] occurrence of the potassium analog of galileiite, $KFe_4(PO_4)_3$ has been located in another IIIA iron meteorite." This is presumably the same material from the Sandtown IIIA iron meteorite whose analysis is reported in Table 2 of Olsen et al. (1999) with a sum of 99.60 wt%, and which yields the empirical formula: $(K_{0.596}Na_{0.390}Ca_{0.017})_{\Sigma 1.003}(Fe_{3.350}Mn_{0.615}Cr_{0.026})_{\Sigma 3.991}P_{2.994}O_{12}$. This K-rich phase has the simplified formula: $(K_{0.6}Na_{0.4})(Fe_{3.4}Mn_{0.6})(PO_4)_3$, and occurs in direct contact with graftonite and johnsomervilleite in the Sandtown IIIA meteorite (Olsen et al. 1999); it probably represents another occurrence of olsenite.

Olsenite and galileiite belong, in the Dana classification, to the Anhydrous Phosphates $(A^+B^{2+})_5(PO_4)_3$, which also includes the recently described triclinic mineral xenophyllite, $Na_4Fe_7(PO_4)_6$, found in the troilite nodules of the Augustinovka IIIAB iron meteorite (Britvin et al. 2020). The Dana numbers of galileiite and xenophyllite are 38.02.05.04 and 38.02.05.05, respectively. Although its crystal structure has not been determined, xenophyllite is probably related structurally to the monoclinic synthetic compounds $RbNa_3Fe_7(PO_4)_6$ and $KNa_3Fe_7(PO_4)_6$; xenophyllite has an *I*-centered subcell that is similar to the primitive unit cell of olsenite (Queen et al. 2007; Britvin et al. 2020). In the Nickel-Strunz classification, galileiite and xenophyllite belong to "Phosphates without additional anions and without H_2O and with medium-sized and large cations" and their Nickel-Strunz numbers are both 08.AC.50 (webmineral.com; accessed July 2022).

Raman spectroscopy

The Raman spectra of elaliite, elkinstantonite, and olsenite were obtained from grains with sizes exceeding 2 µm, ensuring the acquired spectra were devoid of additions from surrounding phases. There is also no indication of Raman modes from the surrounding phases wüstite, troilite, sarcopside, or graftonite in the Raman spectra of the new phosphate minerals. The Raman spectra of each novel mineral exhibit distinctive Raman bands, confirming their unique compositions and crystal structures. The P-O stretching mode between 930 and 1020 cm^{-1} is consistently the strongest and well-defined feature in each spectrum, indicative of a high degree of crystallinity.

The low relative peak intensity of the major modes, high fluorescence background, and lower frequency of the P-O symmetric stretching mode at 937 cm^{-1} in the Raman spectrum of elaliite are likely a result of the elevated Fe-content of the mineral. A broad hump in the bending region at around 488 cm^{-1} may indicate the presence of disorder, mentioned earlier, in the crystal structure of elaliite.

The presence of a triplet in the Raman spectrum of elkinstantonite, instead of a single band observed in the spectra of elaliite and olsenite, is due to either the non-equivalence of the three phosphate groups in the structure, or overtones and/or combination frequencies (Šoptrajatov and Petrov 1967).

Olsenite is the potassium analog of galileiite, and the Raman spectrum of galileiite has a single P-O symmetric stretching band at around 980 cm^{-1}, and weak bands at around 595, 556, 417, and 1125 cm^{-1} (Xie and Chen 2020). Comparing their Raman spectra, both olsenite and galileiite have different stretching and bending modes but both have a similar single band in the P-O symmetric stretch region; for olsenite this mode occurs at lower frequency, probably because of the larger radius of potassium.

Petrogenesis

Phosphate-rich inclusions often occur with troilite in meteorites, e.g., Augustinovka IIIAB (Britvin et al. 2020), Chelyabinsk LL5 chondrite (Sharygin et al. 2016), Darinskoe IIC (Sharygin 2022), Elga IIIE (Litasov and Podgornykh 2017), Graves Nunataks (GRA) 95209 lodranite (Grew et al. 2010), Krymka LL3.1 chondrite (Semenenko and Perron 2005), Sahara 03505 sulfide-rich iron (D'Orazio et al. 2009), and the Yanzhuang H6 chondrite (Xie and Chen 2020). Most occurrences in non-iron meteorites (e.g., chondrites, lodranites) may be attributable to shock metamorphism (e.g., Grew et al. 2010). In iron mete-

orites, iron-rich phosphates are predominantly sarcopside and graftonite; chromite is the most common O-bearing associated mineral (e.g., Olsen et al. 1999; Litasov and Podgornykh 2017). Phosphate minerals vary in composition and identity among iron meteorites, but are commonly Na±Ca±Mg-dominant (e.g., Olsen et al. 1999; Litasov and Podgornykh 2017; Britvin et al. 2020). In the Morasko IAB iron, the main phosphates are buchwaldite ($NaCaPO_4$), brianite [$Na_2CaMg(PO_4)_2$], moraskoite [$Na_2Mg(PO_4)F$], and czochralskiite [$Na_4Ca_3Mg(PO_4)_4$]; these are found in association with Ca-phosphates such as merrillite and fluorapatite (Karwowski et al. 2016; Rubin and Ma 2021). The mineralogy of meteoritic phosphates is reviewed by Olsen et al. (1999) for IIIAB iron meteorites and more broadly by Rubin and Ma (2017, 2021). The observation that phosphate minerals in IIIAB meteorite are carriers of the incompatible lithophile elements Fe, Mn, Na, Ca, Mg, and K (Olsen et al. 1999), appears to be the general case for most inclusions in iron meteorites.

The common paragenesis of the iron phosphates found in the El Ali meteorite—including elaliite, elkinstantonite, olsenite, and graftonite/sarcopside—is in association with wüstite and troilite within inclusions of two general size populations: <200 µm across ("small") and >200 µm across ("large") (Figs. 1–3). The mineral assemblages vary between inclusion types, with small inclusions typically containing troilite + wüstite + elaliite ± elkinstantonite ± sarcopside/graftonite. Large inclusions consist of troilite + wüstite on their margins—wherein wüstite is present as blebs within troilite, and graftonite-rich areas in their cores (Fig. 1). Elaliite in this setting is present at the boundary of these two areas and as small (<10 µm) grains within the graftonite-rich areas, along with small (<10 µm) grains of sarcopside and troilite (Fig. 1, inset). We interpret the texture of the large inclusions as reflecting the solidification of a sulfide-rich melt, with wüstite blebs representing unmixing of an FeO-component from troilite, followed by the solidification of a more O-rich (and S-poor) melt, represented by the graftonite-rich areas. Within this context, elaliite crystallizes at the boundary between these melts and in association with graftonite in the inclusion cores, where the activity of oxygen (the oxygen fugacity) is sufficiently high to form this mixed-valence phosphate. Terrestrial alteration is present in the form of voids lined with hematite (Fig. 1); however, these crosscut the iron phosphate mineral assemblage and, therefore, were not involved in their formation.

In small inclusions, the paragenesis is similar; however, it appears that the melt that solidified in each small inclusion varied in bulk composition, as shown by differences in their mineral assemblages (Figs. 2–3). It is notable that elkinstantonite and olsenite have thus far been found in only one small inclusion each. Elaliite occurs as ~10 µm grains between troilite ± wüstite and elkinstantonite (Fig. 2) and as ~1–2 µm grains included within olsenite or as sub-micrometer inclusions within graftonite/sarcopside (Fig. 3), suggestive of differences in crystallization sequence in different inclusions. We conclude that the mineral assemblage in each inclusion—and therefore the occurrence of elaliite, elkinstantonite, and olsenite—depends on the relative proportions of Fe, S, P, K, Ca, and O trapped within a given inclusion, and the crystallization sequence. In all cases, the system is constrained to low oxygen fugacity by the host iron meteorite.

Implications

All iron oxyphosphate minerals form at relatively high temperatures (pyrometamorphism, granites, and now iron meteorites). Whereas elkinstantonite and olsenite contain only ferrous iron, both ferrous and ferric iron are essential in elaliite. It is probable that the local oxygen fugacity increased as solidification within the sulfide-rich inclusions of the El Ali meteorite proceeded, as elaliite appears to be the last phase to crystallize. All of these new phosphate minerals (elaliite, elkinstantonite, and olsenite) reflect the local chemical conditions of their microenvironments (phosphate-rich areas inside of sulfide inclusions). It is probable that other phosphate-bearing iron meteorites (e.g., Sandtown IIIA, discussed above) may contain a similar low f_{O_2}, high-Fe phosphate assemblage.

Acknowledgments

We dedicate this work to the memory of Erin L. Walton, whose enthusiasm for, and prowess with, the Raman spectrometer inspired many studies of minerals, from high-pressure polymorphs in shock veins to the new minerals described in this study; she will be deeply missed—a bright light gone too soon.

We thank Mark Labbe for the preparation of the type specimen, and Rebecca Funk for searches of the ICDD-PDF4 database. We thank Nick Gessler (Duke University) and numerous contacts within Somalia and elsewhere for providing access to the material used in this research. We thank two anonymous reviewers for detailed comments that resulted in improvements to the manuscript.

Funding

Funding was provided by Natural Sciences and Engineering Research Council of Canada grant RGPIN-2018-04902 to C.D.K.H. SEM-EBSD analyses were carried out at the Caltech GPS Division Analytical Facility, which is supported, in part, by NSF Grants EAR-0318518 and DMR-0080065.

References cited

Anderson, J.B., Shoemaker, G.L., and Kostiner, E. (1978) The crystal structure of $Cu_4(PO_4)_2O$. Journal of Solid State Chemistry, 25, 49–57, https://doi.org/10.1016/0022-4596(78)90042-7.

Armstrong, J.T. (1995) CITZAF: A package of correction programs for the quantitative electron microbeam X-ray-analysis of thick polished materials, thin-films, and particles. Microbeam Analysis, 4, 177–200.

Assaaoudi, H., Fang, Z., Ryan, D.H., Butler, I.S., and Kozinski, J.A. (2006) Hydrothermal synthesis, crystal structure, and vibrational and Mössbauer spectra of a new tricationic orthophosphate $KCo_3Fe(PO_4)_3$. Canadian Journal of Chemistry, 84, 124–133, https://doi.org/10.1139/v05-235.

Attfield, J.P., Cheetham, A.K., Cox, D.E., and Sleight, A.W. (1988) Synchrotron X-ray and neutron powder diffraction studies of the structure of α-$CrPO_4$. Journal of Applied Crystallography, 21, 452–457, https://doi.org/10.1107/S0021889888004625.

Baies, R., Pérez, O., Caignaert, V., Pralong, V., and Raveau, B. (2006) A new sodium cobaltophosphate with a tunnel structure, ionic conductor. Journal of Materials Chemistry, 16, 2434–2438, https://doi.org/10.1039/B516383H.

Barbier, J. and Frampton, C. (1992) The crystal structure of $(Mg,Ga)_8(Ga,Ge)_2O_{12}$. Zeitschrift für Kristallographie, 198, 79–88, https://doi.org/10.1524/zkri.1992.198.1-2.79.

Barbier, J. and Hyde, B.G. (1987) $Mg_7Ga_2GeO_{12}$, a new spinelloid-related compound, and the structural relations between spinelloids (including spinel) and the β-Ga_2O_3 and NaCl types. Acta Crystallographica Section B, 43, 34–40, https://doi.org/10.1107/S0108768187098331.

Bouchdoug, M., Courtois, A., Gerardin, R., Steinmetz, J., and Gleitzer, C. (1982) Preparation et etude d'un oxyphosphate $Fe_4(PO_4)_2O$. Journal of Solid State Chemistry, 42, 149–157, https://doi.org/10.1016/0022-4596(82)90261-4.

Britvin, S., Krivovichev, S., Obolonskaya, E., Vlasenko, N., Bocharov, V., and Bryukhanova, V. (2020) Xenophyllite, $Na_4Fe_7(PO_4)_6$, an exotic meteoritic phosphate: new mineral description, Na-ions mobility and electrochemical implications. Minerals, 10, 300.

Britvin, S.N., Murashko, M.N., Krzhizhanovskaya, M.G., Vapnik, Y., Vlasenko, N.S., Vereshchagin, O.S., Pankin, D.V., and Vasiliev, E.A. (2021a) Moabite, IMA 2020–092. CNMNC Newsletter 60. Mineralogical Magazine, 85, 454–458.

Britvin, S.N., Murashko, M.N., Krzhizhanovskaya, M.G., Vapnik, Y., Vlasenko, N.S., Vereshchagin, O.S., Bocharov, V.N., and Vasiliev, E.A. (2021b) Beershevaite, IMA 2020-095a. CNMNC Newsletter 61. European Journal of Mineralogy, 33, 299–304.

Britvin, S.N., Murashko, M.N., Krzhizhanovskaya, M.G., Vlasenko, N.S., Vereshchagin, O.S., Vapnik, Y., and Bocharov, V.N. (2023) Crocobelonite, $CaFe^{3+}_2(PO_4)_2O$, a new oxyphosphate mineral, the product of pyrolytic oxidation of natural phosphides.

American Mineralogist, 108, 1973–1983, https://doi.org/10.2138/am-2022-8757.
Brunel-Laügt, M., Durif, A., and Guitel, J.C. (1978) Structure cristalline de $Cu_4(PO_4)_2O$. Journal of Solid State Chemistry, 25, 39–47, https://doi.org/10.1016/0022-4596(78)90041-5.
Cipriani, C., Mellini, M., Pratesi, G., and Viti, C. (1997) Rodolicoite and grattarolaite, two new phosphate minerals from Santa Barbara Mine, Italy. European Journal of Mineralogy, 9, 1101–1106, https://doi.org/10.1127/ejm/9/5/1101.
de Faria, D.L.A., Venâncio Silva, S., and De Oliveira, M.T. (1997) Raman microspectroscopy of some iron oxides and oxyhydroxides. Journal of Raman Spectroscopy, 28, 873–878, https://doi.org/10.1002/(SICI)1097-4555(199711)28:11<873:AID-JRS177>3.0.CO;2-B.
Donovan, J.J., Lowers, H.A., and Rusk, B.G. (2011) Improved electron probe microanalysis of trace elements in quartz. American Mineralogist, 96, 274–282, https://doi.org/10.2138/am.2011.3631.
Donovan, J.J., Kremser, D., Fournelle, J.H., and Goemann, K. (2015) Probe for EPMA: Acquisition, automation and analysis, ver. 11. Probe Software, Inc.
D'Orazio, M., Folco, L., Chaussidon, M., and Rochette, P. (2009) Sahara 03505 sulfide-rich iron meteorite: Evidence for efficient segregation of sulfide-rich metallic melt during high-degree impact melting of an ordinary chondrite. Meteoritics & Planetary Science, 44, 221–231, https://doi.org/10.1111/j.1945-5100.2009.tb00730.x.
Droop, G.T.R. (1987) A general equation for estimating Fe^{3+} concentrations in ferromagnesian silicates and oxides from microprobe analyses, using stoichiometric criteria. Mineralogical Magazine, 51, 431–435, https://doi.org/10.1180/minmag.1987.051.361.10.
Dungan, M.A., Donovan, J.J., Locock, A.J., and Bullock, E.S. (2023) Incorporating previously neglected excess oxygen associated with ferric iron in matrix corrections of microprobe data from cubic and rhombohedral Fe-Ti oxides. American Mineralogist, 108, 978–986, https://doi.org/10.2138/am-2022-8447.
Fries, M. and Steele, A. (2018) Raman spectroscopy and confocal Raman imaging in mineralogy and petrography. In J. Toporski, T. Dieing, and O. Hollricher, Eds., Confocal Raman Microscopy. 2nd edition, 209–236. Springer International Publishing.
Frost, R.L., Martens, W., Williams, P.A., and Kloprogge, J.T. (2002) Raman and infrared spectroscopic study of the vivianite-group phosphates vivianite, baricite and bobierrite. Mineralogical Magazine, 66, 1063–1073, https://doi.org/10.1180/0026461026660077.
Gattacceca, J., McCubbin, F.M., Grossman, J., Bouvier, A., Chabot, N.L., D'Orazio, M., Goodrich, C., Greshake, A., Gross, J., Komatsu, M., and others. (2022) The Meteoritical Bulletin, No. 110. Meteoritics & Planetary Science, 57, 2102–2105, https://doi.org/10.1111/maps.13918.
Grew, E.S., Yates, M.G., Beane, R.J., Floss, C., and Gerbi, C. (2010) Chopinite-sarcopside solid solution, $[(Mg,Fe)_3\square](PO_4)_2$, in GRA95209, a transitional acapulcoite: Implications for phosphate genesis in meteorites. American Mineralogist, 95, 260–272, https://doi.org/10.2138/am.2010.3153.
Hatert, F. (2019) A new nomenclature scheme for the alluaudite supergroup. European Journal of Mineralogy, 31, 807–822, https://doi.org/10.1127/ejm/2019/0031-2874.
Hatert, F., Grew, E.S., Vignola, P., Rotiroti, N., Nestola, F., Keller, P., Baijot, M., Bruni, Y., Fransolet, A.-M., Dal Bo, F., and others. (2021) Crystal chemistry and nomenclature of fillowite-type phosphates. Canadian Mineralogist, 59, 781–796, https://doi.org/10.3749/canmin.2000043.
Hellenbrandt, M. (2004) The inorganic crystal structure database (ICSD)—present and future. Crystallography Reviews, 10, 17–22, https://doi.org/10.1080/08893110410001664882.
Holland, T.J.B. and Redfern, S.A.T. (1997) Unit cell refinement from powder diffraction data: The use of regression diagnostics. Mineralogical Magazine, 61, 65–77, https://doi.org/10.1180/minmag.1997.061.404.07.
Karwowski, Ł., Kryza, R., Muszyński, A., Kusz, J., Helios, K., Drożdżewski, P., and Galuskin, E.V. (2016) Czochralskiite, $Na_4Ca_3Mg(PO_4)_4$, a second new mineral from the Morasko IAB-MG iron meteorite (Poland). European Journal of Mineralogy, 28, 969–977, https://doi.org/10.1127/ejm/2016/0028-2557.
Keller, P., Fontan, F., Velasco Roldan, F., and Melgarejo, J.C. (1997) Staněkite, $Fe^{3+}(Mn,Fe^{2+},Mg)(PO_4)O$: A new phosphate mineral in pegmatites at Karibib (Namibia) and French Pyrénées (France). European Journal of Mineralogy, 9, 475–482, https://doi.org/10.1127/ejm/9/3/0475.
Kraus, W. and Nolze, G. (1996) POWDER CELL—a program for the representation and manipulation of crystal structures and calculation of the resulting X-ray powder patterns. Journal of Applied Crystallography, 29, 301–303, https://doi.org/10.1107/S0021889895014920.
Litasov, K.D. and Podgornykh, N.M. (2017) Raman spectroscopy of various phosphate minerals and occurrence of tuite in the Elga IIE iron meteorite. Journal of Raman Spectroscopy, 48, 1518–1527, https://doi.org/10.1002/jrs.5119.
Ma, C. and Rossman, G.R. (2008) Barioperovskite, $BaTiO_3$, a new mineral from the Benitoite Mine, California. American Mineralogist, 93, 154–157.
——— (2009) Tistarite, Ti_2O_3, a new refractory mineral from the Allende meteorite. American Mineralogist, 94, 841–844.
Mandarino, J.A. (1976) The Gladstone-Dale relationship—Part I, derivation of new constants. Canadian Mineralogist, 14, 498–502.
Matvienko, E.N., Yakubovich, O.V., Simonov, M.A., and Belov, N.V. (1981) Crystal structure of K,Fe^{2+}-orthophosphate, $KFe_4[PO_4]_3$. Doklady Akademii Nauk SSSR, 259, 591–595.
Nielsen, C.H. and Sigurdsson, H. (1981) Quantitative methods for electron microprobe analysis of sodium in natural and synthetic glasses. American Mineralogist, 66, 547–552.
Olsen, E.J. and Steele, I.M. (1997) Galileiite: A new meteoritic phosphate mineral. Meteoritics & Planetary Science, 32, A155–A156, https://doi.org/10.1111/j.1945-5100.1997.tb01593.x.
Olsen, E.J., Kracher, A., Davis, A.M., Steele, I.M., Hutcheon, I.D., and Bunch, T.E. (1999) The phosphates of IIIAB iron meteorites. Meteoritics & Planetary Science, 34, 285–300, https://doi.org/10.1111/j.1945-5100.1999.tb01752.x.
Pekov, I.V., Zubkova, N.V., Yapaskurt, V.O., Belakovskiy, D.I., Vigasina, M.F., Sidorov, E.G., and Pushcharovsky, D.Yu. (2014) New arsenate minerals from the Arsenatnaya fumarole, Tolbachik volcano, Kamchatka, Russia. II. Ericlaxmanite and kozyrevskite, two natural modifications of $Cu_4O(AsO_4)_2$. Mineralogical Magazine, 78, 1553–1569, https://doi.org/10.1180/minmag.2014.078.7.03.
Pieczka, A., Hawthorne, F.C., Ball, N., Abdu, Y., Gołębiowska, B., Włodek, A., and Żukrowski, J. (2018) Graftonite-(Mn), ideally $^{M1}Mn^{M2,M3}Fe_2(PO_4)_2$, and graftonite-(Ca), ideally $^{M1}Ca^{M2,M3}Fe_2(PO_4)_2$, two new minerals of the graftonite group from Poland. Mineralogical Magazine, 82, 1307–1322, https://doi.org/10.1180/minmag.2017.081.109.
Queen, W., Hwu, S.-J., and Wang, L. (2007) New low-dimensional iron(II) phosphate exhibiting field-dependent magnetization steps. Angewandte Chemie International Edition, 46, 5344–5347, https://doi.org/10.1002/anie.200604236.
Rubin, A.E. and Ma, C. (2017) Meteoritic minerals and their origins. Chemie der Erde, 77, 325–385, https://doi.org/10.1016/j.chemer.2017.01.005.
——— (2021) Meteorite Mineralogy. Cambridge Planetary Science 26. Cambridge University Press. Online. https://doi.org/10.1017/9781108613767.
Schwunck, H.-M., Moser, P., and Jung, W. (1998) Das Kupfer(II)-oxidphosphat $Cu_4O(PO_4)_2$ in einer neuen, orthorhombischen Modifikation durch Oxidation einer Tl/Cu/P-Legierung. Zeitschrift für Anorganische und Allgemeine Chemie, 624, 1262–1266, https://doi.org/10.1002/(SICI)1521-3749(199808)624:8<1262:AID-ZAAC1262>3.0.CO;2-R.
Semenenko, V.P. and Perron, C. (2005) Shock-melted material in the Krymka LL3.1 chondrite: Behavior of the opaque minerals. Meteoritics & Planetary Science, 40, 173–185, https://doi.org/10.1111/j.1945-5100.2005.tb00373.x.
Sharygin, V.V. (2022) Sodium-rich phosphate and silicate inclusions in the troilite nodule of the Darinskoe iron meteorite (IIC). Geochemistry International, 60, 1221–1236, https://doi.org/10.1134/S0016702922120059.
Sharygin, V.V., Karmanov, N.S., Podgornykh, N.M., and Tomilenko, A.A. (2016) Melt inclusions in impact associations of Chelyabinsk meteorite (Chebarkul fragment). Asian Current Research On Fluid Inclusions (ACROFI-VI), extended abstracts volume, 30–33.
Šoptrajatov, B. and Petrov, I. (1967) On the structure and symmetry of the phosphate ions in some calcium phosphates. Croatica Chemica Acta, 39, 37–45.
Steele, I. and Hutcheon, N. (2020) Memorial of Edward J. Olsen 1927–2020. American Mineralogist, 105, 583–584, https://doi.org/10.2138/am-2020-m697.
Sugiyama, K. and Kimiyama, M. (2009) Crystal structure of ammonium tetrairon trisphosphate(V), $[NH_4][Fe_4(PO_4)_3]$. Zeitschrift für Kristallographie. New Crystal Structures, 224, 369–370, https://doi.org/10.1524/ncrs.2009.0161.
Tait, K.T., Hawthorne, F.C., and Halden, N.M. (2021) Alluaudite-group phosphate and arsenate minerals. Canadian Mineralogist, 59, 243–263, https://doi.org/10.3749/canmin.2000057.
Venturini, G., Courtois, A., Steinmetz, J., Gerardin, R., and Gleitzer, C. (1984) Preparation et étude d'un oxyphosphate de fer à valence mixte $Fe_9(PO_4)O_8$. Journal of Solid State Chemistry, 53, 1–12, https://doi.org/10.1016/0022-4596(84)90222-6.
Volkova, L.M. (2023) Orthorhombic and triclinic modifications of the arsenate $Cu_4O(AsO_4)_2$ and isotypic phosphates $Cu_4O(PO_4)_2$: Strongly frustrated antiferromagnetics. Physica Scripta, 98, 025824.
Wasson, J.T. and Kallemeyn, G.W. (2002) The IAB iron-meteorite complex: A group, five subgroups, numerous grouplets, closely related, mainly formed by crystal segregation in rapidly cooling melts. Geochimica et Cosmochimica Acta, 66, 2445–2473, https://doi.org/10.1016/S0016-7037(02)00848-7.
Xie, X. and Chen, M. (2020) Fe-Mn-Na phosphates and Al-free chromite in the metal-troilite eutectic nodule. In X. Xie and M. Chen, Eds., Yanzhuang Meteorite: Mineralogy and Shock Metamorphism, 167–204. Springer.
Yakubovich, O., Kiriukhina, G., Shvanskaya, L., Maximova, O., Volkov, A., Dimitrova, O., Ovchenkov, E., Yumashev, O., Iqbal, A., Rahaman, B., and others. (2018) Canted antiferromagnet superimposed on a buckled kagomé network in $RbMn_4(PO_4)_3$. Acta Crystallographica Section C, 74, 641–649, https://doi.org/10.1107/S2053229618006034.
Zhang, H., Zhao, Y., Wen, M., Dong, Y., Fan, Q., Kuang, Q., Liu, H., and Lian, X. (2018) A new sodium ferrous orthophosphate $Na_4Fe_4(PO_4)_3$ as anode materials for sodium-ion batteries. Journal of Materials Science, 53, 8385–8397, https://doi.org/10.1007/s10853-018-2128-4.

Manuscript received October 13, 2023
Manuscript accepted March 15, 2024
Accepted manuscript online March 28, 2024
Manuscript handled by Antonio M. dos Santos